EXPLOITING THE LOW-RANK PROPERTY OF HYPERSPECTRAL IMAGERY: A TECHNICAL OVERVIEW

Hongyan Zhang [1,2*], *Wei He* [2], *Wenzhi Liao* [1], *Renbo Luo* [1], *Liangpei Zhang* [2], *Aleksandra Pižurica* [1]

[1] Ghent University-TELIN-IPI-iMinds, Ghent, Belgium
[2] State Key Lab. of Inf. Eng. in Surveying, Mapping and Remote Sensing, Wuhan University, China
zhanghongyan@whu.edu.cn

ABSTRACT

Hyperspectral images (HSIs) often suffer from various annoying degradations, which poses huge challenges for the practical applications. Fortunately, clean HSI is intrinsically low-rank, which opens up a broad category of HSI processing and analysis methods with high robustness against the complicated mixture of various noises and outliers. Based on the low rank property of HSI, this paper provides a comprehensive review on restoration, multi-angle registration and unmixing methods for HSIs developed very recently, and insights for further investigations.

***Index Terms*—** Low-rank, hyperpsectral image, restoration, registration, unminxing

1. INTRODUCTION

Hyperspectral imaging sensors, which combine the imaging and spectroscopy science together, provide up to nm-level spectral resolution and diagnostic spectral feature, supporting the improved analysis tasks [1], such as classification, unmixing, target detection and so on. Therefore, with the fine spectral discrimination, hyperspectral images (HSIs) have been widely used in various fields, including earth observation, environmental monitoring, food analysis, criminal identification and so on.

However, on the other hand, assuming that the spatial resolution is fixed, due to the pursuit of high spectral resolution, the energy used to produce each hyperspectral band, which spans a narrow wavelength range, is limited. As a result, the useful imaging information can be easily overwhelmed by various kinds of noise [2], such as Gaussian noise and impulse noise. In addition, dead pixel/line and stripes commonly exist in HSIs because of the failure or abnormal response of the sensor device. Most of the traditional HSI restoration methods fail in practice because they typically assume only one or two kinds of noise, while the actual noise is more complex, which negatively affects the performance of HSI analysis tasks.

In very recent years, the low-rank model achieved great success because of its powerful ability to find and exploit the intrinsic low-dimensional structure of high dimensional data [3]. As HSIs are typically volumetric data of high dimension, the low-rank model is feasible for the HSI tasks and helps to improve the robustness against the various noises. Therefore, this paper reviews the low-rank based HSI processing and analysis methods developed recently, including restoration, multi-angle registration and unmixing, and points out the potential further investigations.

2. TECHNICAL BACKGROUND

2.1. Low-rank Matrix Recovery (LRMR) Model

The LRMR model was originally proposed by Wright *et al*. [4], and further improved by Candes *et al.* [3] with the idealization as a "robust principal component analysis" (RPCA) problem. Assuming that a low-rank matrix $\mathbf{L} \in \mathbb{R}^{m\times n}$ is corrupted by a gross sparse error matrix $\mathbf{S} \in \mathbb{R}^{m\times n}$ and a small entry-wise Gaussian noise matrix $\mathbf{N} \in \mathbb{R}^{m\times n}$, then the observed data matrix $\mathbf{D} \in \mathbb{R}^{m\times n}$ can be decomposed as the sum of a Gaussian matrix, a sparse matrix and a low-rank matrix, that is:

$$\mathbf{D} = \mathbf{L} + \mathbf{S} + \mathbf{N} \tag{1}$$

The LRMR model aims at recovering the clean low-rank matrix $\mathbf{L}$ from the contaminated observations $\mathbf{D}$, and can be formulated as:

$$\min_{\mathbf{L},\mathbf{S}} \quad rank(\mathbf{L}) + \lambda \|\mathbf{S}\|_0 \quad s.t \quad \|\mathbf{D}-\mathbf{L}-\mathbf{S}\|_F \le \delta \tag{2}$$

where δ is a constant related to the standard deviation of random noise $\mathbf{N}$, and λ is the regularization parameter used to tradeoff the relative contributions.

Due to the high non-convexity of the optimization problem, it is common to relax (2) by replacing the ℓ_0-norm with the ℓ_1- norm, and the rank measure with the nuclear norm [4], respectively, which yields the following convex surrogate:

$$\min_{\mathbf{L},\mathbf{S}} \quad \|\mathbf{L}\|_* + \lambda \|\mathbf{S}\|_1 \quad s.t \quad \|\mathbf{D}-\mathbf{L}-\mathbf{S}\|_F \le \delta \tag{3}$$

The optimization problem (3) can be effectively solved with the inexact augmented Lagrange multiplier (ALM) method [6] or the "Go Decomposition" (GoDec) algorithm [7].

2.2 Low-rank Property of Clean HSI

The baseline of the low-rank based HSI analysis tasks attributes to the low-rank property of the clean HSI, which can be exploited from the perspective of a linear spectral mixing model [8], [9]. The linear mixing model attempts to decompose the clean HSI matrix into a product of a pure spectral endmember matrix and an abundance matrix.

Assuming that the clean HSI without any noise with the size of $M \times N \times B$ is lexicographically reordered as a 2-D matrix $\mathbf{X} \in \mathbb{R}^{B \times MN}$, and denoting the spectral endmember matrix and the abundance matrix as $\mathbf{A} \in \mathbb{R}^{B \times K}$ and $\mathbf{C} \in \mathbb{R}^{K \times MN}$, respectively, the linear mixing model can be formulated as:

$$\mathbf{X} = \mathbf{AC} \tag{4}$$

where M, N and B denote the height, width and band number of the HSI, and K represents the number of spectral endmembers. As the upper bound value of the number of endmembers K is usually relatively small, then the rank of the matrix $\mathbf{X}$ is bounded, i.e., $rank(\mathbf{X}) \le K \ll \min(B, MN)$, which explicitly suggests the low-rank property of the clean HSI.

3. LOW-RANK BASED HSI PROCESSING AND ANALYSIS METHODS

3.1 HSI Restoration

Here we consider four kinds of noise involved in the corruption of HSI, including Gaussian noise, impulse noise, dead pixels or lines, and stripes. Firstly, we build up the HSI degradation model, which models the HSI imaging process and describe the mathematical relationship between the desired clean HSI image and the observed one. Ideally, the HSI degradation model can be given as:

$$\mathbf{Y} = \mathbf{X} + \mathbf{E} + \mathbf{N} \tag{5}$$

where $\mathbf{Y}$, $\mathbf{E}$ and $\mathbf{N}$ denote the lexicographically reordered version of the observed HSI, the combination of impulse noise, dead pixels or lines, and stripes, and Gaussian noise, respectively.

It is apparent that there exists high similarity between the LRMR model (1) and the HSI degradation model (5). With the low-rank property of the clean HSI, the matrix $\mathbf{X}$ is clearly low-rank. Fortunately, as the impulse noise, dead pixels or lines, and stripes only corrupt some parts or some bands of the HSI, the matrix $\mathbf{E}$ is sparse. So, it is natural to apply sparse and low-rank matrix decomposition (3) to the noisy matrix $\mathbf{Y}$ and obtain the clean HSI $\mathbf{X}$ [9].

Comparing with the traditional HSI restoration methods, the LRMR method achieves outstanding denoising performance [10]. However, the LRMR method mainly relies on the high correlation between spectral bands, and lacks appropriate spatial constraints [10]. Therefore, various approaches have been reported to improve the LRMR model from different perspectives [10]-[13]. A notable representative is the total-variation-regularized low-rank matrix factorization (LRTV) method [11], which improves the LRMR method by imposing the TV regularization across the spatial domain, and can be formulated as:

$$\begin{aligned} \min_{\mathbf{X},\mathbf{S} \in \mathbb{R}^{m \times n}} & \|\mathbf{X}\|_* + \tau \|\mathbf{X}\|_{HTV} + \lambda \|\mathbf{E}\|_1 \\ s.t & \|\mathbf{Y} - \mathbf{E} - \mathbf{S}\|_F^2 \le \delta, rank(\mathbf{X}) \le r \end{aligned} \tag{6}$$

where $\|\mathbf{X}\|_{HTV}$ represents the hyperspectral total variation model, and $rank(\mathbf{X})$ is added to explicitly constrain the number of the endmembers. The ALM method can be utilized to resolve the optimization model (6) [5], [11].

3.2 Multi-angle HSI Registration

As a prerequisite of all applications, the registration of multi-angle HSI (MA-HSI) faces the problem of effective feature extraction and the robustness to degradations and occlusions. Here all the angle images of the same earth surface are denoted as $\mathbf{D}=[\mathbf{Y}_0, \mathbf{Y}_1, \ldots, \mathbf{Y}_s]$ with $\mathbf{Y}_0$ denoting the reference nadir image, where $s+1$ denotes the number of angles. Assuming that $\mathbf{H}_1, \ldots, \mathbf{H}_s$ denotes the optimal spatial transformations of $\mathbf{Y}_1, \ldots, \mathbf{Y}_s$ with respect to the reference image $\mathbf{Y}_0$, they can be transformed into the coordinate system of the reference image. The matrix version of the well-registered MA-HSI is formulated:

$$\mathbf{A} = \mathbf{D} \circ \mathbf{H} = [\mathbf{X}_0^T \,|\, \mathbf{X}_1^T \circ \mathbf{H}_1 \,|\, \cdots \,|\, \mathbf{X}_s^T \circ \mathbf{H}_s] \in \mathbb{R}^{MN \times ((s+1) \times B)} \tag{6}$$

where $\mathbf{H}$ is a general term for all the transformation parameters. It is clear that the stacked version well-registered MA-HSI $\mathbf{A}$ is also low-rank.

Therefore, with low-rank constraint as the registration feature, the robust registration for MA-HSI can be transformed to solve the set of transformations $\mathbf{H}$ by optimizing the following rank minimization problem, termed robust registration rank minimization (RRRM) [14]:

$$\min_{\mathbf{A},\mathbf{H}} \; rank(\mathbf{A}) \quad s.t. \; \mathbf{D} \circ \mathbf{H} = \mathbf{A} \tag{7}$$

Considering the degradations and occlusions brought by different imaging angles between the MA-HSIs, the optimization model can be modified as follows:

$$\min_{\mathbf{A},\mathbf{E},\mathbf{H}} \; \|\mathbf{A}\|_* + \gamma \|\mathbf{E}\|_1 \quad s.t. \; \|\mathbf{D} \circ \mathbf{H} - \mathbf{A} - \mathbf{E}\|_F \le \varepsilon \tag{8}$$

The ALM optimization method can be adopted to solve the model (8) after linearization [14].

3.3 HSI Unmixing

To alleviate the negative influence of the sparse noise for unmixing, it is natural to integrate the sparse noise detection and hyperspectral unmixing (HU) in a unified framework. By integrating (4) and (5), we can obtain the

(a) (b) (c) (d) (e)

Fig. 1. Restoration results of band 187 in the urban image data experiment: (a) original, (b) SSAHTV, (c) VBM3D, (d) LRMR and (e) LRTV.

extended linear mixing model with the consideration of sparse noise:

$$\mathbf{Y} = \mathbf{AC} + \mathbf{E} + \mathbf{N} \tag{9}$$

With this model in mind, the generalized robust HU model can be formulated as [15]:

$$\min_{\mathbf{A},\mathbf{C},\mathbf{E}} \frac{1}{2} \| \mathbf{Y} - \mathbf{E} - \mathbf{AC} \|_F^2 + \lambda t(\mathbf{E}) + \beta h(\mathbf{A}) + \gamma g(\mathbf{C}) \tag{10}$$

where $t(\bullet)$ is the sparsity-inducing function which promotes the detection and removal of the sparse noise, $h(\bullet)$ and $g(\bullet)$ denote the suitable constraints on the endmember matrix **A** and abundance matrix **S**, respectively.

As a specification of model (10), $\|\bullet\|_{1,2}$ and $\|\bullet\|_{1/2}$ are utilized to induce the removal of noise and the sparsity of abundance fraction, so the $L_{1/2}$-norm regularized robust non-negative matrix factorization ($L_{1/2}$-RNMF) method was presented and expressed as [15]:

$$\min_{\mathbf{A},\mathbf{C},\mathbf{E}} \frac{1}{2} \| \mathbf{Y} - \mathbf{E} - \mathbf{AC} \|_F^2 + \lambda \|\mathbf{E}\|_{1,2} + \gamma \| \mathbf{C} \|_{1/2} \; s.t. \; \mathbf{A} \geq 0, \mathbf{C} \geq 0 \tag{11}$$

The extended multiplicative iterative algorithm can be utilized to simultaneously solve the endmember matrix **A** and abundance matrix **C**.

As another instantiation, with the available spectral library as the prior endmember dictionary, Aggarwal *et. al.* built the robust sparse HU model in the presence of mixed noise as [16]:

$$\min_{\mathbf{C},\mathbf{E}} \frac{1}{2} \| \mathbf{Y} - \mathbf{E} - \mathbf{AC} \|_F^2 + \lambda \|\mathbf{E}\|_1 + \gamma \| \mathbf{C} \|_{2,1} + \beta \| \nabla \mathbf{C} \|_1 \tag{12}$$

where $\|\mathbf{C}\|_{2,1}$ and $\|\nabla \mathbf{C}\|_1$ denote joint sparsity and total variation constraint on the abundance matrix **C**, respectively. The split-Bregman approach can be used to retrieve the abundance fraction [16].

4. EXPERIMENTAL RESULTS AND DISCUSSIONS

4.1 HSI Restoration

The HYDICE urban image with the size of $307 \times 307 \times 210$ is utilized in our HSI restoration experiment. All the water absorption bands (104–108, 139–151, and 207–210) are removed, leaving 162 low-noise bands and 27 high-noise bands [15]. The SSAHTV [17], and VBM3D [18], LRMR [9] and LRTV [11] methods are selected for comparisons. The experimental results are illustrated in Fig.1. It can be clearly observed that the VBM3D method cannot remove the stripes. The SSAHTV method can remove the stripes to a certain extent, but causes the restoration results to be over-smooth. The LRMR and LRTV methods can both simultaneously remove the stripes and preserve the image details, and LRTV further improves the results of LRMR by imposing the spatial constraints. More experimental results and quantitative evaluations can be found in [8], [10], and [13].

4.2 MA-HSI Registration

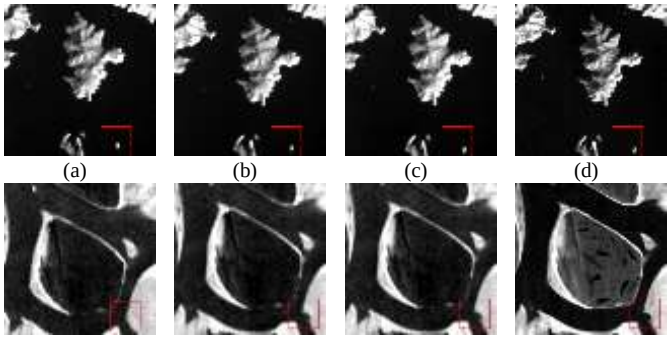

(a) (b) (c) (d)

(e) (f) (g) (h)

Fig. 2. Details of the registration results by the different methods. The first row CHRIS_FY and second row CHRIS_UK. From the first column to the last: SIFT+NCC, MANUAL, RRRM, and the reference image, respectively.

TABLE I
COMPARISON OF CC AMONG THE DIFFERENT METHODS

Site	Angle	SIFT+NCC	MANUAL	RRRM
CHRIS_ FY	+36°	0.9306	0.9546	**0.9714**
	−36°	0.9278	0.9659	**0.9783**
	+55°	0.9073	0.9179	**0.9739**
	−55°	0.9141	0.9482	**0.9685**
CHRIS_ UK	+36°	0.9364	0.9589	**0.9736**
	−36°	0.9385	0.9667	**0.9780**
	+55°	0.9026	0.9191	**0.9687**
	−55°	0.9240	0.9434	**0.9779**

Two sets of 5 angle CHRIS/Proba image are utilized in the MA-HSI registration experiment, which are termed CHRIS_FY and CHRIS_UK both with 18 spectral bands, 17 m nadir resolution and size of 748×744. The $0°$ angle image is chosen as the reference image, and the remaining four angle images are selected as the sensed ones to be registered. The RRRM method [14], the SIFT+NCC

method in [19] and the MANUAL method based on visual inspection are selected as comparison methods. The experimental results and quantitative evaluations are shown in Fig.2 and TABLE I, respectively. In each row of TABLE I, the best results for the quality index are labeled in bold, and the second best results are underlined. From the image details shown in the red square box, it can be observed that the RRRM method outperforms SIFT+NCC and can achieve almost the same effect as the MANUAL method from visual comparison. From TABLE I, it can be observed that the quantitative evaluation results are consistent with the visual comparisons and RRRM generally achieves better results in all angles. More experimental results and quantitative evaluations can be found in [14].

4.3 HSI Unmixing

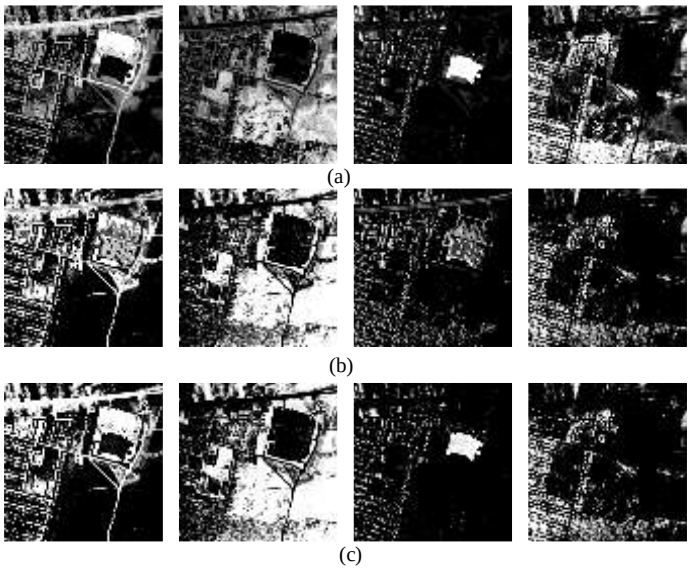

Fig. 3. Abundance maps of each endmembers using different methods with the 189 noisy bands. From the first row to the last: benchmark, $L_{1/2}$-NMF and $L_{1/2}$-RNMF. From the first column to the last: asphalt, grass, roof and tree.

TABLE II.
SAD VALUES OF THE DIFFERENT METHODS WITH THE NOISY IMAGE.

	$L_{1/2}$-RNMF	$L_{1/2}$-NMF	rNMF	EDCNMF	SISAL
Asphalt	<u>0.0844</u>	0.0948	**0.0767**	0.1001	0.2144
Grass	**0.0786**	<u>0.0918</u>	0.1579	0.1055	0.2320
Roof	**0.0652**	0.1746	0.3982	0.2418	<u>0.1083</u>
Tree	**0.0692**	<u>0.1028</u>	0.1401	0.1413	0.1592
Mean	**0.0744**	<u>0.1160</u>	0.1932	0.1472	0.1785

The HYDICE urban image with 162 low-noise and 27 high-noise bands is used in the HSI unmixing experiment. There exist four types of land covers: asphalt, grass, roof and tree. The benchmark abundance maps of each signature shown in Fig. 3(a) were achieved via the method in [20]. Fig. 3 (b) and (c) shows the unmixing results of $L_{1/2}$ regularized NMF and RNMF, respectively, which clearly shows the superiority of the $L_{1/2}$-RNMF method over the $L_{1/2}$-NMF method with the consideration of the negative effect of the sparse noise. Table II gives the mean SAD values obtained by the $L_{1/2}$-RNMF method and several other state-of-the-art unminxing methods to present the quantitative evaluations, including robust NMF (rNMF) [21], endmember dissimilarity constrained NMF [22] (EDCNMF), and simplex identification via split augmented Lagrangian (SISAL) [23]. In each row of TABLE II, the best results for the quality index are labeled in bold, and the second best results are underlined. It can be observed that $L_{1/2}$-RNMF method achieves the best quantitative results. More experimental results and quantitative evaluations can be found in [15].

5. CONCLUSIONS AND FUTURE DIRECTIONS

Based on the inherent low-rank property of clean HSI, this paper provides an overview of the robust HSI restoration, registration and unmixing methods. By modeling the sparse noise and outliers with one sparse matrix implanted within the corresponding HSI analysis framework, the robustness can be greatly improved. The further investigations mainly focus on better modelling of HSI noise and the exploitation of new related applications, such as super-resolution, fusion, classification, change detection and so on.

6. REFERENCES

[1] A. Plaza, J. A. Benediktsson, J. W. Boardman, J. Brazile, L. Bruzzone, G. Camps-Valls, J. Chanussot, M. Fauvel, P. Gambah, A. Gualtieri, M. Marconcini, J. C. Tilton, and G. Trianni, "Recent advances in techniques for hyperspectral image processing," *Remote Sens. Environ.*, vol. 113, no. 1, pp. S110–S122, Sep. 2009.

[2] H. Zhang, H. Shen, L. Zhang, "A Super-Resolution Reconstruction Algorithm for Hyperspectral Images", *Signal Process.*, vol. 92, no. 9, pp. 2082-2096, 2012.

[3] E. J. Candes, X. Li, Y. Ma, and J. Wright, "Robust principal component analysis?," *J. ACM*, vol. 58, no. 3, May 2011.

[4] J. Wright, A. Ganesh, S. Rao, Y. Peng, and Y. Ma, "Robust principal component analysis: Exact recovery of corrupted low-rank matrices via convex optimization," in *Proc. NIPS*, 2009, pp. 2080–2088.

[5]E. J. Candes, and T. Tao, "The power of convex relaxation: Near-optimal matrix completion," *IEEE Trans. Inf. Theory*, vol. 56, no. 5, pp. 2053–2080, May 2010.

[6] Z. Lin, M. Chen, and Y. Ma, "The augmented lagrange multiplier method for exact recovery of corrupted low-rank matrices," *Arxiv preprint* arXiv:1009.5055, 2009.

[7] T. Zhou, and D. Tao, "Godec: Randomized low-rank & sparse matrix decomposition in noisy case." in *Proc. 28th ICML*, 2011, pp. 33–40.

[8] M. Golbabaee, and P. Vandergheynst, "Hyperspectral image compressed sensing via low-rank and joint-sparse matrix recovery." in *Proc. IEEE ICASSP*, 2012, pp. 2741–2744.

[9] H. Zhang, W. He, L. Zhang, H. Shen, Q. Yuan, "Hyperspectral Image Restoration Using Low-Rank Matrix Recovery", *IEEE Trans. Geosci. Remote Sens.*, vol. 52, no. 8, pp. 4729-4743, 2014.

[10] M. Wang, J. Yu, J.-H. Xue, W. Sun, "Denoising of Hyperspectral Images using Group Low-rank Representation", *IEEE J. Sel. Topics Appl. Earth Obs. Remote Sens.*, DOI: 10.1109/JSTARS.2016.2531178, 2016.

[11] W. He, H. Zhang, L. Zhang, H. Shen, "Total-Variation-Regularized Low-rank Matrix Factorization for Hyperspectral Image Restoration", *IEEE Trans. Geosci. Remote Sens.*, vol. 54, no. 1, pp. 178 - 188, 2016.

[12] Zhu, R., Dong, M. and Xue, J.-H, "Spectral Non-local Restoration of Hyperspectral Images with Low-rank Property". *IEEE J. Sel. Topics Appl. Earth Obs. Remote Sens.*, vol. 8, no.6, pp. 3062-3067, 2015.

[13] W. He, H. Zhang, L. Zhang, H. Shen, "Hyperspectral Image Denoising via Noise-Adjusted Iterative Low-Rank Matrix Approximation", *IEEE J. Sel. Topics Appl. Earth Obs. Remote Sens.*, vol. 8, no. 6, pp. 3050 - 3061, 2015.

[14] T. Hu, H. Zhang, H. Shen, L. Zhang, "Robust Registration by Rank Minimization for Multiangle Hyper/Multispectral Remotely Sensed Imagery", *IEEE J. Sel. Topics Appl. Earth Obs. Remote Sens.*, vol. 7, no. 6, pp. 2443 - 2457, 2014.

[15] W. He, H. Zhang, L. Zhang, "Sparsity-Regularized Robust Non-Negative Matrix Factorization for Hyperspectral Unmixing", *IEEE J. Sel. Topics Appl. Earth Obs. Remote Sens.*, DOI: 10.1109/JSTARS.2016.2519498, 2016.

[16] H. K. Aggarwal, A. Majumdar, "Hyperspectral Unmixing in the Presence of Mixed Noise using Joint-Sparsity and Total-Variation", *IEEE J. Sel. Topics Appl. Earth Obs. Remote Sens*., DOI: 10.1109/JSTARS.2016.2521898, 2016.

[17] Q. Yuan, L. Zhang, and H. Shen, "Hyperspectral Image Denoising Employing a Spectral-Spatial Adaptive Total Variation Model," *IEEE Trans. Geosci. Remote Sens.*, vol. 50, no. 10, pp. 3660-3677, Oct 2012.

[18] K. Dabov, A. Foi, and K. Egiazarian, "Video denoising by sparse 3D transform-domain collaborative filtering," *presented at the Eur. Signal Processing Conf.*, Poznan, Poland, Sep. 2007.

[19] J. Ma, J. C.-W. Chan, and F. Canters, "Fully Automatic Subpixel Image Registration of Multiangle CHRIS/Proba Data," *IEEE Trans. Geosci. Remote Sens.*, vol. 48, no. 7 pp. 2829–2839, Jul. 2010.

[20] F. Zhu, Y. Wang, B. Fan, S. Xiang, G. Meng, and C. Pan, "Spectral Unmixing via Data-Guided Sparsity," *IEEE Trans. Image Process.* , vol. 23, pp. 5412-5427, Dec. 2014.

[21] C. Fevotte and N. Dobigeon, "Nonlinear hyperspectral unmixing with robust nonnegative matrix factorization," *IEEE Trans. Image Process.*, vol. 24, no. 12, pp. 4810–4819, Dec. 2015.

[22] N. Wang, B. Du, and L. Zhang, "An endmember dissimilarity constrained non-negative matrix factorization method for hyperspectral unmixing," *IEEE J. Sel. Topics Appl. Earth Observ. Remote Sens.*, vol. 6, no. 2, pp. 554–569, Apr. 2013.

[23] J. M. Bioucas-Dias, "A variable splitting augmented Lagrangian approach to linear spectral unmixing," in *Proc. 1st Workshop Hyperspectr. Image Signal Process.: Evol. Remote Sens. (WHISPERS'09)*, 2009.